Hisactophilin-Mediated Binding of Actin to Lipid Lamellae: A Neutron Reflectivity Study of Protein Membrane Coupling

Christoph Naumann,* Christian Dietrich,* Almuth Behrisch,* Thomas Bayerl,# Michael Schleicher,§ David Bucknall,¶ and Erich Sackmann*

*Physik Department, E22 (Biophysical Laboratory), Technische Universität München, D-85747 Garching, Germany; #Fakultät für Physik, Universität Würzburg, Physikalisches Institut EP-5, Am Hubland, 97047 Würzburg, Germany; §Institut für Zellbiologie, Fakultät für Medizin, Ludwig Maximilian Universität München, 80336 München, Germany; and ¶Rutherford Appleton Laboratory, Chilton, Didcot, Oxon OX11 0QX, England

ABSTRACT The neutron reflectivity technique is applied to determine the adsorptive interaction of the 13.5-kDa actin-binding protein hisactophilin from *Dictyostelium discoideum* with lipid monolayers at a lateral pressure of 21 mN/m $\leq \pi \leq$ 25 mN/m at the air-water interface. We compare binding of natural hisactophilin exhibiting a myristic acid chain membrane anchor at the N-terminus (DIC-HIS) and a fatty acid-deficient genetic product expressed in *Escherichia coli* (EC-HIS). It is demonstrated that only the natural hisactophilin DIC-HIS is capable of mediating the strong binding of monomeric actin to the monolayer, where it forms a layer of about 40 Å thickness corresponding to the average diameter of actin monomers. Monolayers composed of pure dimyristoyl phosphatidylcholine with fully deuterated hydrocarbon tails and headgroup (DMPC-d67) and 1:1 mixtures of this lipid with chain deuterated dimyristoyl phosphatidylglycerol (DMPG-d54) are studied on subphases consisting either of fully deuterated buffer (D_2O) or of a 9:1 H_2O/D_2O buffer that matches the scattering length density of air (CMA buffer). The reflectivity data are analyzed in terms of layer models, consisting of one to three layers, depending on the contrast of the buffer and the system. We show that both protein species bind tightly to negatively charged 1:1 DMPC-d67/DMPG-d54 monolayers, thereby forming a thin and most probably monomolecular protein layer of 12–15 Å thickness. We find that the natural protein (DIC-HIS) partially penetrates into the lipid monolayer, in contrast to chain-deficient species (EC-HIS), which forms only an adsorbed layer. The coverage of the monolayer with DIC-HIS strongly depends on the presence of anionic DMPG in the monolayer. At a bulk protein concentration of 1.5 μg/ml, the molar ratio of bound protein to lipid is about 1:45 for the 1:1 lipid mixture but only 1:420 for the pure DMPC.

GLOSSARY

R	specular reflectivity
Q	momentum transfer of specularly reflected beam
Θ_g	grazing angle of incidence
n	neutron refractive index
b_i	scattering length of nuclei i
ρ_i	scattering length density of layer i
d_i	thickness of layer i
σ_i	interfacial roughness of layer i
A_L	average area per lipid molecule
A_p	average area per adsorbed protein molecule
A_p(NMR)	area per adsorbed protein molecule determined by NMR measurements

INTRODUCTION

The mechanism of binding of the actin-based cytoskeleton to membranes is still widely unknown, particularly the requirement and the role of membrane-spanning receptors like those of the integrin family. Recently, substantial evidence has been provided that two types of actin-binding proteins are involved in the cytoskeleton-membrane coupling, namely talin and hisactophilin. Both proteins are able to mediate directly the coupling of actin filaments to lipid lamellae containing charged lipids (Kaufmann et al., 1992; Dietrich et al., 1993; Behrisch et al., 1995).

Talin is a large (230 kDa) cytosolic protein that is accumulated near the inner leaflet of the cell plasma membrane (particularly at the leading edge of pseudopods) and is (together with vinculin and most probably receptors of the integrin family) involved in the formation of focal contacts (Isenberg and Goldmann, 1995; Goldmann et al., 1994; Samuels et al., 1993).

Hisactophilin is a small, roughly cylindrical, 13.5-kDa polypeptide exhibiting at one face three histidin-rich loops, and both C- and N- terminal ends at the other. A myristic acid chain is coupled to the N-terminus on the top of a β-barrel structure (Hanakam et al., 1995). The histidin-rich face provides the binding site for actin, and the fatty acid is supposed to facilitate the membrane anchoring.

In recent phenomenological surface-sensitive measurements (film balance, microfluorescence), evidence was provided for the following (Behrisch et al., 1995):

1) membrane binding of hisactophilin is mediated by electrostatic forces;

2) proteins partially penetrate into the semipolar monolayer surface;

3) the fatty acid chain is required for the functional orientation of the actin monomer-binding protein.

Received for publication 11 July 1995 and in final form 28 April 1996.

Address reprint requests to Dr. Erich Sackmann, Physik Department, E22 (Biophysical Laboratory), Technische Universität München, James-Franck-Strasse, D-85747 Garching, Germany; Tel.: 49-89-28912471; Fax: 49-89-28912469; E-mail: sackmann@physik.tu-muenchen.de.

Abbreviations used: DIC-HIS, natural hisactophilin from *Dictyostelium discoideum* cells; EC-HIS, hisactophilin expressed in *E. coli*; DMPC-d67, dimyristoyl phosphatidylcholine with deuterated hydrocarbon chains and choline headgroups; DMPG-d54, chain deuterated dimyristoyl phosphatidylglycerol.

0006-3495/96/08/811/13 $2.00

To gain more insight into structural aspects of hisactophilin membrane coupling and hisactophilin-mediated binding of actin to membranes, we performed neutron reflectivity measurements. By exploiting the unique possibilities of scattering contrast variation, this technique enables high-precision measurements of both the molecular mass density distribution in the direction normal to the monolayer surface and the layer thicknesses (Penfold and Thomas, 1989; Russell, 1990; Bayerl et al., 1990; Johnson et al., 1991b; Vaknin et al., 1991; Brumm et al., 1994; Naumann et al., 1994, 1995). One major advantage of the neutron reflectivity technique is its high sensitivity, requiring only a few tens of micrograms of proteins per experiment.

In the present work we studied the coupling of natural hisactophilin from *Dictyostelium discoideum* and the same protein produced by genetic expression in *E. coli* bacteria to partially charged lipid monolayers kept at high lateral pressures (21 mN/m $\leq \pi \leq$ 25 mN/m). Because the genetic product (Scheel et al., 1989) lacks the myristic acid chain, the role of hydrophobic chains for membrane binding of water-soluble proteins could be simultaneously explored. Additionally, we investigate the influence of electrostatic forces caused by the charged lipids of the monolayer for the membrane coupling of DIC-HIS and EC-HIS. Direct evidence is provided that the fatty acid-containing protein partially penetrates into the membrane and can mediate the tight binding of monomeric actin to membranes. In contrast, the chain-deficient species adsorbs only and does not couple monomeric actin to membrane.

MATERIALS AND METHODS

Materials

Dimyristoyl phosphatidylcholine, with both the fatty acids and the headgroup deuterated and glycerol backbone protonated (DMPC-d67), as well as dimyristoyl phosphatidylglycerol (DMPG-d54), in which only the chains are deuterated, were purchased from Avanti Polar Lipids (Alabaster, AL). Heavy water was purchased from Deuchem (Leipzig, Germany). Natural hisactophilin was isolated from starved *Dictyostelium discoideum* cells following the procedure by Stöckelhuber et al. (unpublished results). The genetic product denoted as EC-HIS was expressed in *Escherichia coli* following the procedure described by Scheel et al. (1989).

The various lipid samples were spread onto an aqueous solution (subphase), containing 10 mM HEPES buffer, 10 mM NaCl, 0.25 mM EDTA, and 0.25 mM EGTA. Different pH values were adjusted by the addition of NaOH. Two different pH values were used (pH 6 and pH 9). All experiments were performed at 20°C.

Neutron reflectivity experiments

All experiments were performed with the CRISP spectrometer (Penfold and Thomas, 1989) at the Rutherford Appleton Laboratories (Didcot, England).

The film balance attached to the spectrometer was described in detail previously (Naumann et al., 1994). For the present experiments a small Teflon trough (surface area, 64.55 cm^2; subphase volume, 40 ml) was inserted into the large trough (15 × 45 × 0.5 cm^3) in such a way that the monolayers spread on the water surface of the outer and inner compartments were interconnected by a thin channel (1.5 × 0.5 cm^2 surface, 0.4 cm depth). After the lipid monolayer was spread and the lateral pressure was adjusted, the channel between the two compartments was closed and the proteins were injected into the subphase of the insert by syringes. The lateral pressure was measured in the small compartment by a Wilhelmy system (accuracy: 0.1 mN/m). CRISP operates at a fixed grazing angle of incidence of $\theta_G = 1.5°$. The intensity of the specular reflected neutrons is analyzed as a function of the momentum transfer Q

$$Q = 4\pi \sin \theta_G/\lambda \tag{1}$$

by the time-of-flight technique. The available wavelength range of CRISP of 0.5–6.5 Å corresponds to a Q range of 0.05 $Å^{-1} \leq Q \leq 0.65$ $Å^{-1}$. The incoherent background for each sample, which is uniform over the measured Q range, was determined by extrapolation to high values of the momentum transfer Q. It was subtracted from the measured reflectivity $R(Q)$, and the difference was then processed as described below. The Q-dependent specular reflectivity $R(Q)$ is determined by spatial variation of the scattering length density distribution, $\rho(z)$, in direction normal to the interface. More precisely, $R(Q)$ is proportional to the Fourier transform of the first derivative of $\rho(z)$ (Als-Nielsen, 1985):

$$R(Q) \propto \left| \int \left(\frac{\partial \rho}{\partial z} \right) e^{iQz} \, dz \right|^2. \tag{2}$$

However, owing to the close analogy to the specular reflection of light, $R(Q)$ can be analyzed using Fresnel's law of optical reflection by representing the complex interface as a stratified film exhibiting sharp interfaces between layers of different refractive index n_i (Penfold and Thomas, 1989; Russell, 1990). The latter is related to the neutron scattering length density ρ_i by

$$n_i = 1 - \frac{\lambda^2 \cdot \rho_i}{2\pi}, \tag{3}$$

whereas ρ_i is directly related to the atom number densities $N_{i\alpha}$:

$$\rho_i = \sum_\alpha N_{i\alpha} \cdot b_\alpha, \tag{4}$$

where b_α is the scattering length of atoms of type α. The reflectivity curves $R(Q)$ are most conveniently analyzed in terms of the well-known optical matrix method (Born and Wolf, 1970; cf. Bayerl et al., 1990, for further references).

We investigated the lipid/protein coupling by considering the following systems:

deuterated lipid on a subphase of D_2O buffer
deuterated lipid on a subphase of CMA buffer (contrast matched to air)
deuterated lipid and protonated protein on a subphase of D_2O buffer
deuterated lipid and protonated protein on a subphase of CMA buffer.

A schematic illustration of both contrasts in the presence of the proteins is shown in Fig. 1.

Procedure of data analysis

The key strategy for analysis of the mass density distribution in the normal direction of the layer system is a systematic application of contrast variation procedures by partial deuteration of the lipid and/or of the subphase combined with simulations of the reflectivity curves for the various scenarios. The simplest model for the interpretation of the data are a two-box model for the case of the lipid/protein layer on D_2O buffer and a three-box model for the lipid/protein layer on CMA buffer. The major problem is that the two-layer model is determined by four parameters and the three-layer model by six parameters. Without additional information about the structural parameter of the lipid and other constraints, the data analysis of the $R(Q)$-versus-Q curves would not yield a unique set of parameters. We therefore adopted the following procedure of data analysis:

1) Each experiment of lipid/protein coupling was started by recording reflectivity-versus-Q curves for the pure lipid monolayer, which was maintained at the same lateral pressure as in the presence of the protein. Small

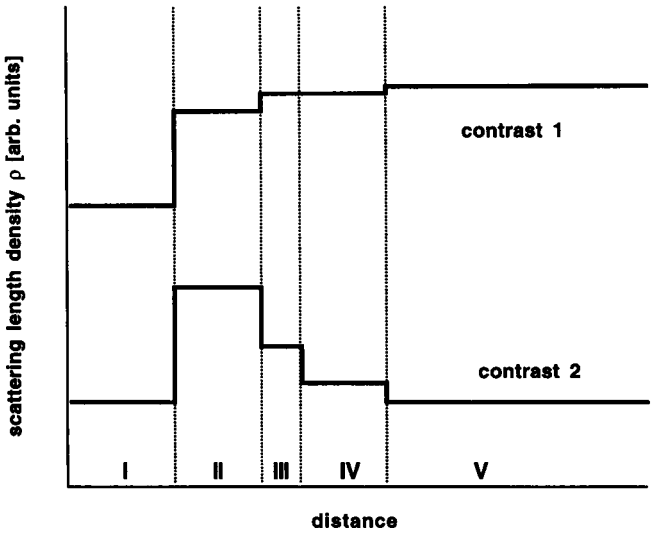

FIGURE 1 Schematic view of contrast variation of deuterated lipid/protonated protein on D_2O buffer (contrast 1) and of deuterated lipid/protonated protein on CMA buffer (contrast 2) in direction normal to the membrane. The numbers I-V correspond to the following regions: I, air; II, lipid chains (deuterated); III, lipid headgroup (deuterated/protonated); IV, protein (protonated); V, subphase (D_2O buffer or CMA buffer).

variations of the lateral pressure from experiment to experiment thus did not affect the change of the layers by protein adsorption.

The reflectivity curves can be interpreted in terms of a one-layer model in the case of a deuterated lipid monolayer on D_2O, because the contrast between bulk water and the headgroup region is very small (cf. contrast 1 in Fig. 1). The fitting of the experimental $R(Q)$-versus-Q curve by two free parameters (namely, the scattering length density and the thickness) leads to a unique result.

In case of the deuterated lipid monolayer on CMA buffer, the monolayer has to be described by a two-box model (cf. contrast 2 in Fig. 1), which implies four parameters (two values of scattering length density and the thickness of each layer). We take into account that the molecular area obtained from the fitted parameters A_L(NR) must agree with the molecular area A_L(FB) measured independently by a film balance experiment. By taking into account this constraint, one has only two free parameters (thickness of each layer), which leads again to a unique solution. The validity of this procedure was checked in several previous studies (Naumann et al., 1994, 1995).

2) In the case of the lipid/protein systems, we have to make two further assumptions:

The first is that the addition of hisactophilin does not cause a change in the thickness of the lipid layer.

The second assumption is that only the hydrophobic anchor of the cytosolic protein DIC-HIS is able to penetrate into the hydrophobic interior of the lipid monolayer. If we assume that a lipid monolayer with an area per molecule of about 60 Å^2 is saturated with hisactophilin, which exhibits an area of about A_P = 1000 Å^2 (Habazettl et al., 1992), about one myristic acid chain of DIC-HIS should be present for each 17 phospholipid molecules. The incorporation of protonated protein chain into the fully deuterated lipid chain interior should therefore cause a maximum decrease in scattering length density of the hydrophobic membrane region of $\Delta\rho = 0.17 * 10^{-6}$ Å^{-2}. We therefore conclude that addition of DIC-HIS decreases the scattering length density of the hydrophobic interior of the lipid by not more than $\Delta\rho = 0.2 * 10^{-6}$ Å^{-2}.

For the lipid/protein layers on both D_2O buffer and CMA buffer, we are therefore able to take this value of $\Delta\rho$ as a restricted parameter exhibiting a range of variations of $\Delta\rho \leq 0.2 * 10^{-6}$ Å^{-2}. To take into account incorporation of the myristic acid chain of DIC-HIS, we varied this parameter by incremental steps of $\Delta\rho = 0.1 * 10^{-6}$ Å^{-2}.

Based on the above procedures, the following fixed and restricted parameters are used:

For lipid/protein layers on D_2O buffer (cf. contrast 1 in Fig. 1), we must consider one restricted parameter (scattering length density of the hydrophobic region of the lipid) and one fixed parameter (thickness of the hydrophobic region of the lipid). The reflectivity data of lipid/protein layers on CMA buffer (cf. contrast 2 in Fig. 1) can be accounted for by one restricted parameter (scattering length density of the hydrophobic region of the lipid) and two fixed parameters (thickness of the lipid chain region and thickness of the hydrophilic moiety of the lipid).

In summary, there remain two free-floating parameters for the case of the lipid/protein layer on the D_2O subphase and three free parameters for the lipid/protein layer on CMA buffer. The free parameters obtained by fitting the $R(Q)$-versus-Q curves and the corresponding statistical errors are summarized in Table 1. The statistical errors are obtained by a systematic χ^2 analysis of each free-floating parameter, taking into account that all free-floating parameters depend on each other. The χ^2 plots that are included in the figures show two-dimensional sections through the global minimum. Following the procedure described by Vaknin et al. (1991), we adopt a limit of confidence of 10%.

In some cases (e.g., in the presence of G-actin) the $R(Q)$-versus-Q curves could not be fitted by the above procedure in a satisfactory way. The fitting could, however, be considerably improved by considering contribution by the interfacial roughness σ_i. The following procedure was applied:

1) Each experiment was first analyzed by neglecting interfacial roughness as described above ($\sigma_i = 0$).

2) The original fitting parameters were kept constant while the interfacial roughnesses σ_i were varied until best fit was achieved.

3) Subsequently, the original parameters were varied again while the σ_i were kept constant.

4) We repeatedly applied procedures 2) and 3) successively until the minimum of the χ^2 parameter was achieved.

A systematic error (χ^2) analysis showed that the interfacial roughness can be detected to an accuracy of $\Delta\sigma_i = \pm 3$ Å (cf. Fig. 9).

RESULTS

Pure lipid monolayers

Several neutron reflectivity studies of pure lipid monolayers and lipid mixtures have been reported previously (Bayerl et al., 1990; Vaknin et al., 1991; Johnson et al., 1991b; Brumm et al., 1994; Naumann et al., 1994, 1995). They show that the technique allows reliable measurements of the thicknesses and the scattering length densities of the hydrocarbon

TABLE 1 Free-floating parameters with corresponding statistical errors for deuterated lipid/protonated protein on D_2O buffer and deuterated lipid/protonated protein on CMA buffer

Subphase	Free-floating parameters	Statistical error
D_2O	Thickness of the layer consisting of protein and lipid headgroup	±2 Å
	Scattering length density of the layer consisting of protein and lipid headgroup	$\pm 0.05 * 10^{-6}$ Å^{-2}
CMA	Scattering length density of lipid headgroup	$\pm 0.2 * 10^{-6}$ Å^{-2}
	Thickness of protein layer	±4 Å
	Scattering length density of protein layer	$\pm 0.1 * 10^{-6}$ Å^{-2}

The statistical errors are obtained by systematic χ^2 analysis of each free-floating parameter taking into account that all of these parameters are connected.

and headgroup regions of lipid monolayers as a function of both lateral pressure and phase state of the lipid layers.

Table 2 summarizes the layer thicknesses and the corresponding scattering length densities of pure DMPC-d67 and 1:1 DMPC-d67/DMPG-d54 mixtures used for the present study of protein-lipid interaction.

The data of Table 2 show:

1) In pure D_2O, the monolayer of the 1:1 mixture of DMPC-d67 and DMPG-d54 can be well represented by a single-layer model within the present degree of accuracy. This is caused by the small scattering contrast between the hydrophilic region of the monolayer and subphase (cf. contrast 1 in Fig. 1). The layer thickness corresponds approximately to the hydrophobic region of the lipid monolayer (thickness of $d_1 = 14 \pm 1$ Å and scattering length density of $\rho_1 = 5.5 \pm 0.1 * 10^{-6}$ Å^{-2}). This is in good agreement with values obtained in former experiments (Brumm et al., 1994; Naumann et al., 1994).

2) In the case of the CMA buffer, the monolayer of the 1:1 mixture of DMPC-d67 and DMPG-d54 should be described by a two-layer model. In addition to the large contrast caused by the deuterated lipid chains, there is also a pronounced difference between the scattering length densities of the lipid headgroup and the subphase (cf. contrast 2 in Fig. 1). Therefore more detailed structural information can be obtained for the two moieties of the monolayer.

The changes in the scattering length density of the tail ρ_1 for the different measurements (cf. lines 4 and 5 in Table 2) are due to different lateral pressures. Thus for 21 mN/m the scattering length density is $\rho_1 = 5.5 \pm 0.1 * 10^{-6}$ Å^{-2}, whereas at 25 mN/m, $\rho_1 = 6.0 \pm 0.1 * 10^{-6}$ Å^{-2}.

The value of the scattering length density of $\rho_2 = 3.5 \pm 0.1 * 10^{-6}$ Å^{-2} of the headgroup region of the 1:1 mixture is the algebraic mean of the values for deuterated DMPC-d67 and protonated DMPG-d54 lipids.

The values of the thicknesses of the tail region ($d_1 = 14 \pm 1$ Å) and headgroup region ($d_2 = 9 \pm 1$ Å) agree well with those obtained by previous reflectivity studies of lipid monolayers and supported bilayers deposited by vesicle fusion (Johnson et al., 1991a,b; Brumm et al., 1994; Naumann et al., 1994).

Effect of membrane binding of hisactophilin

In Fig. 2 we show as an example the changes of the reflectivity-versus-Q curves for the monolayer of a 1:1 mixture of DMPC-d67 and DMPG-d54 on the D_2O subphase caused by the binding of the natural DIC-HIS. Best fits for the pure lipid (*dashed line*) and the lipid/protein system (*solid line*) are shown. To simplify the representation, the data points of pure lipid are not shown. Comparison of the two reflectivity curves demonstrates the effect of the protein layer on the reflectivity in the observed range of momentum transfer Q (0.05 Å$^{-1} \leq Q \leq 0.3$ Å^{-1}). The binding of the protein leads to a decrease in reflectivity at $Q \leq 0.09$ Å^{-1} and a shoulder at 0.09 Å$^{-1} \leq Q \leq 0.2$ Å^{-1} (cf. Fig. 2). Further evidence for the binding of DIC-HIS is provided by the χ^2 plot (cf. Fig. 2, *inset*) of the layer thickness d_2 (layer consists of lipid headgroup and protein), which shows a clear minimum at $d_2 = 25 \pm 2$ Å. Taking into account a layer thickness of the lipid headgroup of about 10 Å, we obtain a layer thickness of the bounded protein of 15 ± 2 Å.

Modifications of reflectivity curves caused by binding of natural hisactophilin DIC-HIS (Fig. 3) and the myristic acid-deficient protein EC-HIS (Fig. 4) are exhibited for the monolayer of 1:1 mixed DMPC-d67/DMPG-d54 on a CMA subphase. Simultaneously, optimal fits for the pure lipid (*dashed line*) and lipid/protein system (*solid line*) are shown. Both figures demonstrate the influence of the protein coupling on the reflectivity behavior. The coupling of the natural protein DIC-HIS is indicated by a decreased reflectivity at 0.05 Å$^{-1} \leq Q \leq 0.2$ Å^{-1} (cf. Fig. 3). The binding of the fatty acid-deficient EC-HIS is accompanied by a remarkable change of slope of the reflectivity curve between 0.05 Å$^{-1} \leq Q \leq 0.2$ Å^{-1} (cf. Fig. 4). The insets in Fig. 3 and Fig. 4 show χ^2 plots of the layer thickness of the protein d_3, providing evidence for the binding of both DIC-HIS ($d_3 = 12 \pm 4$ Å) and EC-HIS ($d_3 = 10 \pm 4$ Å) on negatively charged membranes. Both values are in good agreement with the layer thickness of DIC-HIS of 15 ± 2 Å found for 1:1 mixed DMPC-d67/DMPG-d54 plus DIC-HIS on the D_2O subphase.

To investigate the influence of the membrane charge on the process of protein coupling, we also used a monolayer of pure zwitterionic DMPC-d67. In Fig. 5 we show the corresponding reflectivity curves in the absence (*dashed line*) and the presence (*solid line*) of DIC-HIS. In contrast to the experiments with the negatively charged lipid monolayer (cf. Figs. 2–4), Fig. 5 shows only a small change of the reflectivity behavior due to the addition of the protein. Although the change is

TABLE 2 Fitted parameters of layer thicknesses d_i and scattering length densities ρ_i of pure lipid monolayers in D_2O buffer and CMA buffer

System	Buffer	No. of layers	d_1 [Å]	ρ_1 [$*10^{-6}$ Å^{-2}]	d_2 [Å]	ρ_2 [$*10^{-6}$ Å^{-2}]
DMPC-d67/DMPG-d54 (1:1)	D_2O	1	14	5.5	—	—
DMPC-d67	CMA	2	15	6.4	10.9	3.2
DMPC-d67/DMPG-d54 (1:1)	CMA	2	14	5.5	8.8	3.5
DMPC-d67/DMPG-d54 (1:1)	CMA	2	14	6.0	9.9	3.3

All measurements were performed at pH 6.

The indices 1 and 2 denote the hydrophobic chain region and the hydrophilic headgroup region of the lipid monolayer, respectively.

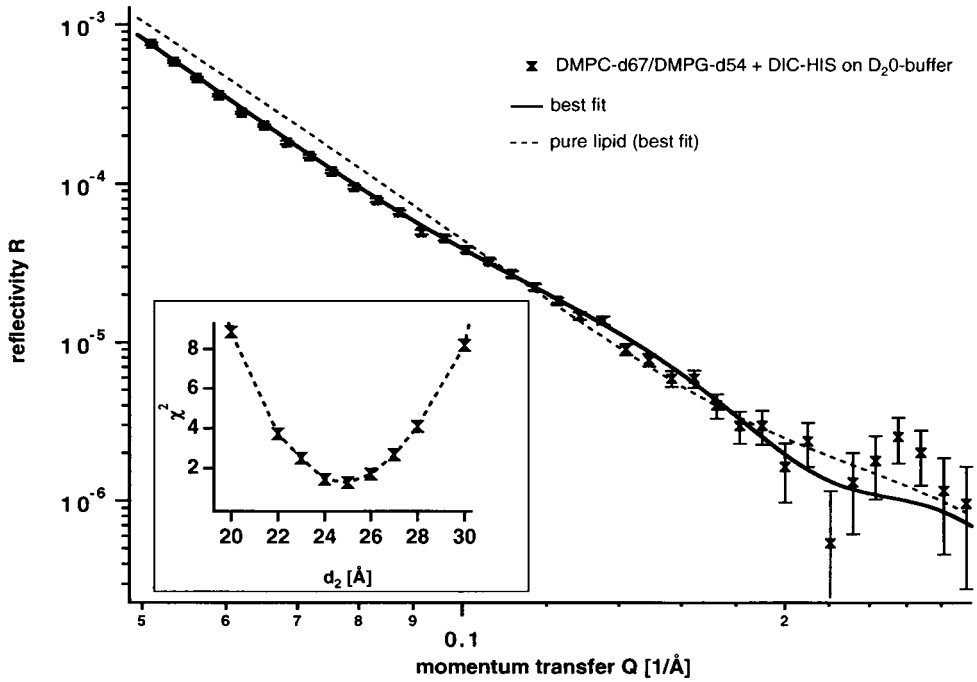

FIGURE 2 Variation of neutron reflectivity $R(Q)$ with momentum transfer Q for monolayer of 1:1 mixture of DMPC-d67/DMPG-d54 in the presence of 0.11 μM DIC-HIS on D_2O buffer at pH 6. Markers indicate experimental data. The drawn line corresponds to the fitting of the experimental data by a two-layer model. The dashed line shows the fitting curve obtained for the lipid monolayer alone. To simplify the representation, the data points of pure lipid are not shown. The layer thicknesses d_i and scattering length densities ρ_i corresponding to the fitting curves are summarized in Table 3. The inset shows the result of the χ^2 analysis of the layer thickness consisting of lipid headgroup and protein, which leads to a systematic error of ± 2 Å.

small, it appreciably exceeds the experimental accuracy, because the minimum of the χ^2 parameter is $\chi^2 = 1.68$, by assuming that DIC-HIS does not bind, whereas $\chi^2 = 1.41$ if binding is assumed (cf. Fig. 5, *inset*).

In Table 3, we summarize the layer thicknesses d_i and the average scattering length densities ρ_i, obtained by our fitting procedures (cf. Materials and Methods). In the presence of the proteins, all reflectivity curves of 1:1 mixture of DMPC-d67/DMPG-d54 are fitted either by a three-layer model (in the case of CMA buffer) or by a two-layer model (in the case of D_2O buffer). Note that for the D_2O subphase, index 1 denotes the hydrophobic region of the lipid monolayer and index 2 the sum of the lipid headgroup layer and the protein layer. For CMA buffer the indices 1, 2, and 3 denote the hydrocarbon region of the lipid layer, the headgroup region of the lipid layer, and the protein layer, respectively.

Table 3 leads to the following conclusions:

1) The fitted values of layer 2 (in the case of D_2O buffer) and layer 3 (in the case of CMA buffer) show that

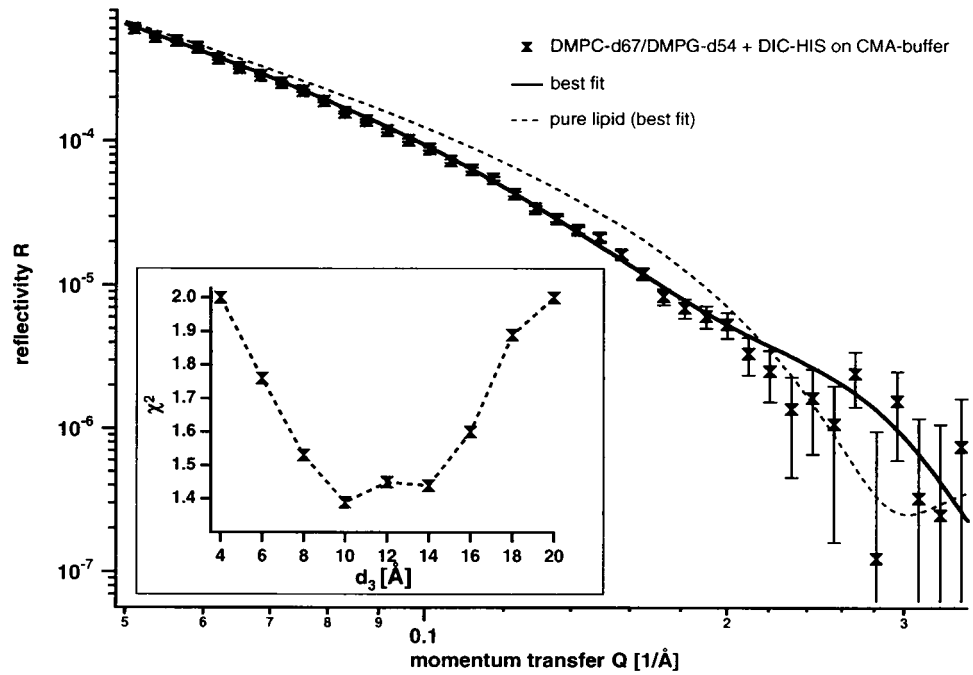

FIGURE 3 Plot of reflectivity $R(Q)$ versus momentum transfer Q (marker) and fitting curve (full line) for 1:1 mixture of DMPC-d67/DMPG-d54 in the presence of 0.11 μM natural protein DIC-HIS in CMA buffer at pH 6. The fitting curve obtained for the pure lipid monolayer (dashed line) is shown for comparison. To simplify the representation, the data points of pure lipid are not shown. The layer thicknesses d_i and scattering length densities ρ_i corresponding to the fitting curves are summarized in Table 3. The inset shows the result of the χ^2 analysis of the protein layer thickness, which leads to a systematic error of ± 4 Å.

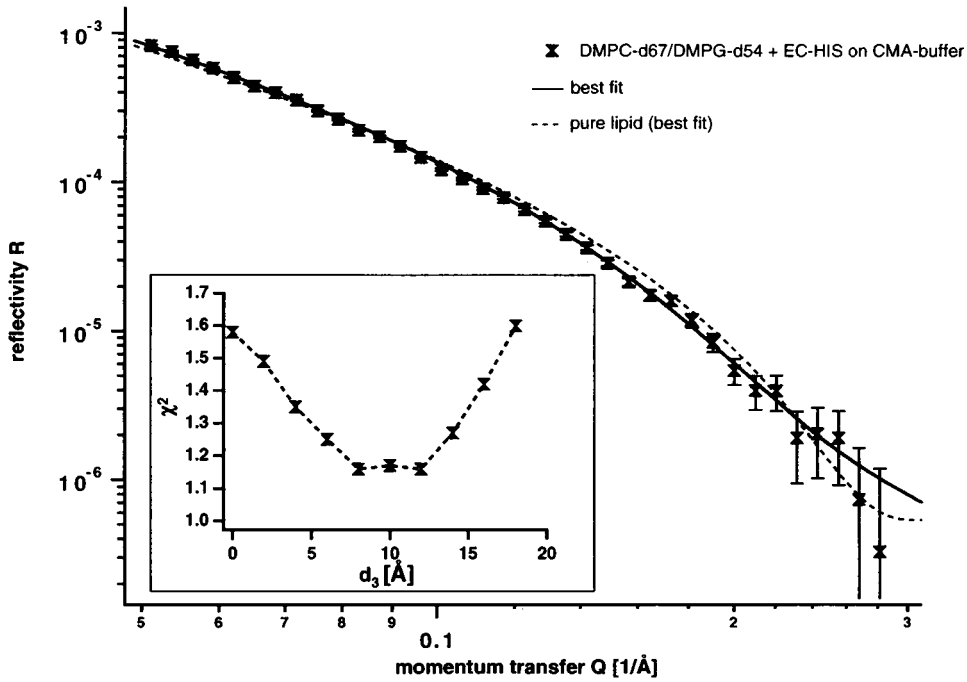

FIGURE 4 Plot of reflectivity $R(Q)$ versus momentum transfer Q (marker) and fitting curve (full line) for 1:1 mixture of DMPC-d67/DMPG-d54 in the presence of 0.11 μM fatty acid-deficient protein EC-HIS on CMA buffer at pH 6. The fitting curve obtained for the pure lipid monolayer (dashed line) is shown for comparison. To simplify the representation, the data points of pure lipid are not shown. The layer thicknesses d_i and scattering length densities ρ_i corresponding to the fitting curves are summarized in Table 3. The inset shows the result of the χ^2 analysis of the protein layer thickness, which leads to a systematic error of ± 4 Å.

both types of proteins (DIC-HIS and EC-HIS) bind to the negatively charged 1:1 DMPC-d67/DMPG-d54 monolayer. We find a protein layer thickness of $d_3 = 10$–15 Å (accuracy: $\Delta d_3 = \pm 4$ Å), which corresponds well to a monomolecular layer of hisactophilin (Habazettl et al., 1992).

2) In agreement with the previous monolayer study of Behrisch et al. (1995), our data provide evidence for the binding of DIC-HIS to DMPC-d67 by the finding that the scattering length density of the headgroup region is remarkably decreased by $\Delta\rho_2 = 0.3 * 10^{-6}$ Å^{-2}, which is comparable to the reduction of $\Delta\rho_2 = 1.0 * 10^{-6}$ Å^{-2}, as found for the partially charged membrane. This leads to the conclusion that the strength of the interaction of the protein with the semipolar head group region of the membrane does not depend on the charge of the bilayer, whereas the lateral concentration of the bound protein is much smaller for the neutral than for the charged membrane. The electrostatic interaction thus facilitates protein binding and leads to the accumulation of proteins at the membrane surface. A more quantitative evaluation of the concentration of adsorbed protein is given below.

3) By assuming that hisactophilin forms a cylinder, we can estimate the average area occupied by one protein A_P as follows. From the values of total scattering length of hisactophilin, fitted scattering length density ρ_3, and thickness d_3 we can determine A_P by the following equation:

$$A_P = \frac{b(\mathrm{HIS})}{d_3\rho_3}. \qquad (5)$$

From the known sequence of amino acids (Scheel et al., 1989) we obtain the total scattering length of the hisactophilin molecule $b(\mathrm{HIS}) = 377 * 10^{-4}$ Å. With this value we obtain the following values of average area per hisactophilin molecule:

DMPC-d67 + DIC-HIS: $A_P \approx 25{,}000$ Å^2

DMPC-d67/DMPG-d54 + DIC-HIS: $A_P \approx 2{,}850$ Å^2

DMPC-d67/DMPG-d54 + EC-HIS: $A_P \approx 4{,}750$ Å^2.

The area per hisactophilin molecule can be estimated to $A_P(\mathrm{NMR}) = 1000$ Å^2 from the structural data provided by the NMR structural determination (Habazettl et al., 1992). With these data we can now calculate the fraction of lipid area φ_P covered by protein according to

$$\varphi_P = \frac{A_P(\mathrm{NMR}) * 100\%}{A_P}. \qquad (6)$$

The following values are obtained:

DMPC-d67 + DIC-HIS: $\varphi_P = 4\%$

DMPC-d67/DMPG-d54 + DIC-HIS: $\varphi_P = 35\%$

DMPC-d67/DMPG-d54 + EC-HIS: $\varphi_P = 21\%$.

An interesting result is the large difference in φ_P of DIC-HIS for charged and noncharged monolayers. It demonstrates the important contribution of electrostatic forces for the accumulation of charged proteins at membrane surfaces and supports the results that were previously published by Behrisch et al. (1995). It leads to the conclusion that electrostatic forces are essential for the enrichment of proteins at membrane surface, but they do not affect the penetration of the protein into the lipid layer.

4) A remarkable difference between the binding mechanisms of natural and fatty acid-depleted proteins is found if

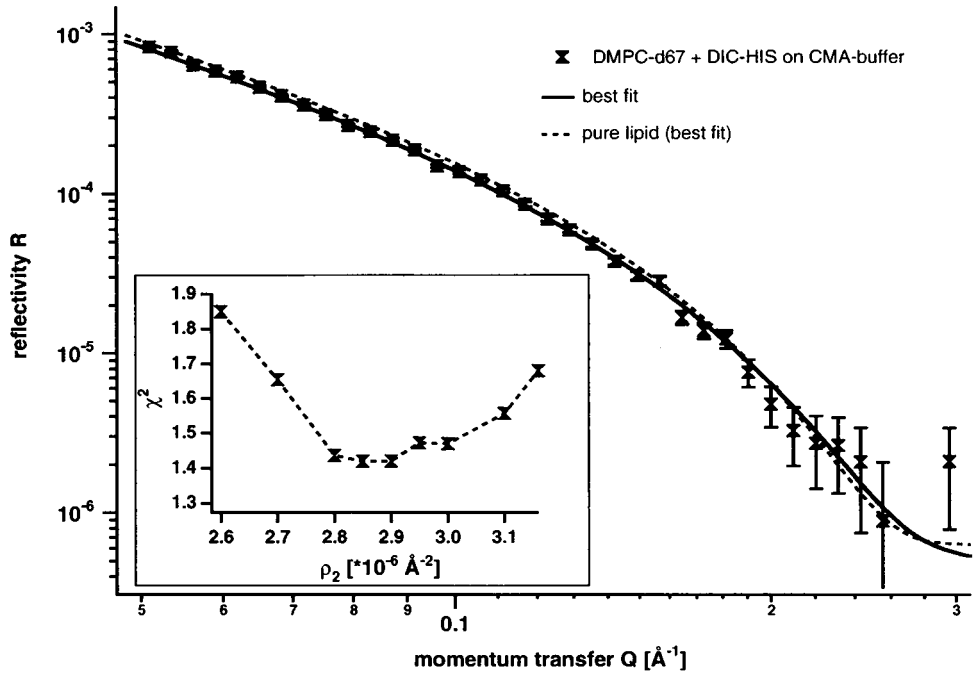

FIGURE 5 Plot of reflectivity $R(Q)$ versus momentum transfer Q (marker) and fitting curve (full line) for DMPC-d67 in the presence of 0.11 μM natural protein DIC-HIS in CMA buffer at pH 6. The fitting curve obtained for the pure lipid monolayer (dashed line) is shown for comparison. To simplify the representation, the data points of pure lipid are not shown. The layer thicknesses d_i and scattering length densities ρ_i corresponding to the fitting curves are summarized in Table 3. The inset shows the result of the χ^2 analysis of the scattering length density of the lipid headgroup, which leads to a systematic error of $\pm 0.2 * 10^{-6}$ Å^{-2}.

one compares scattering length densities of the lipid headgroup ρ_2 for the 1:1 mixed lipid layer on CMA buffer. Whereas DIC-HIS reduces ρ_2 from $\rho_2 = 3.5 \pm 0.2 * 10^{-6}$ Å^{-2} in the absence of the protein to $\rho_2 = 2.5 \pm 0.2 * 10^{-6}$ Å^{-2} in the presence of the protein, the EC-HIS does not effect these parameters within experimental error. Before and after the addition of the protein, we find $\rho_2 = 3.3 \pm 0.2 * 10^{-6}$ Å^{-2} (cf. column ρ_2 in Table 3). This strongly suggests that the fatty acid-deficient protein adsorbs to the lipid layer but does not penetrate. In contrast, the natural form (DIC-HIS) containing the fatty acid chain penetrates, remarkably, into the semipolar region of the lipid layer. The decrease in ρ_2 by about 30% provides strong evidence that side chains of amino acids of DIC-HIS penetrate into the headgroup region of the lipid layer.

This important result is confirmed in Figs. 6 and 7, in which we compare the changes of the $R(Q)$-versus-Q plots for a 1:1 mixture of DMPC-d67 and DMPG-d54 on CMA buffer induced by the two protein species.

The $R(Q)$-versus-Q plot in Fig. 6 (for the EC-HIS) is either fitted by assuming penetration (*dashed line*) or only adsorption (*solid line*) of the myristic acid-deficient protein. Only the latter case yields good fitting results, which demonstrates that the protein EC-HIS adsorbs to the monolayer but does not penetrate.

In Fig. 7, the experimental data for the DIC-HIS are fitted by a model assuming penetration (*solid line*) and a model without penetration (*dashed line*), respectively. Optimal fitting is only achieved for the former case, demonstrating remarkable penetration of the natural protein (DIC-HIS) into the semipolar region of the membrane.

5) The decrease in ρ_1 due to the addition of DIC-HIS points to a partial penetration of the protonated myristic acid chain of DIC-HIS into the deuterated hydrocarbon

TABLE 3 Comparison of fitted parameters of layer thicknesses d_i and scattering length densities ρ_i of DMPC-d67 and 1:1 mixtures of DMPC-d67 and DMPG-d54 before and after binding natural hisactophilin (DIC-HIS) and of the genetic product (EC-HIS)

System	Protein	Buffer	No. of layers	d_1 [Å]	ρ_1 [$*10^{-6}$ Å^{-2}]	d_2 [Å]	ρ_2 [$*10^{-6}$ Å^{-2}]	d_3 [Å]	ρ_3 [$*10^{-6}$ Å^{-2}]
DMPC-d67	—	CMA	2	15	6.4	10.9	3.2	—	—
	DIC-HIS	CMA	3	15	6.3	10.9	2.9	12	0.15
DMPC-d67 + DMPG-d54	—	CMA	2	14	5.5	8.8	3.5	—	—
	DIC-HIS	CMA	3	14	5.4	8.8	2.5	12	1.1
	—	CMA	2	14	6.0	9.9	3.3	—	—
	EC-HIS	CMA	3	14	6.0	9.9	3.3	10	0.8
	—	D_2O	1	14	5.5	—	—	—	—
	DIC-HIS	D_2O	2	14	5.4	25	5.9	—	—

Data are shown for D_2O buffer and CMA buffer at pH6. In the case of the CMA buffer the indices 1–3 denote the lipid chain, the lipid headgroup, and the hisactophilin layer, respectively.

In the case of the D_2O contrast the index 1 denotes the hydrophobic chain region of the lipid monolayer. The index 2 denotes the layer, which consists

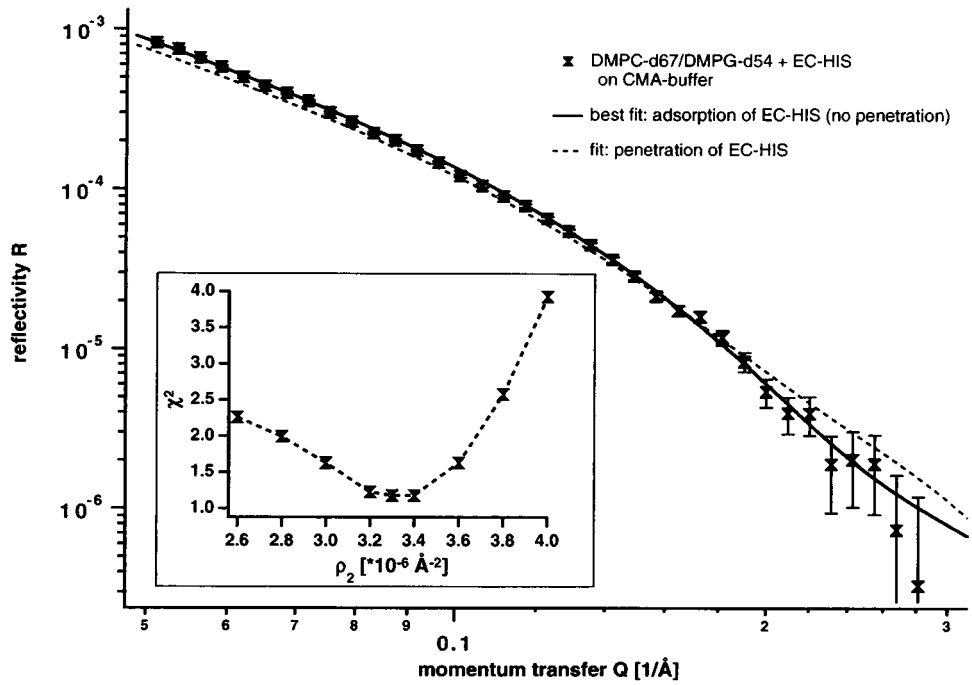

FIGURE 6 Comparison of optimal fits of $R(Q)$-versus-Q curves of EC-HIS on 1:1 mixed DMPC-d67/DMPG-d54 monolayers on CMA buffer at pH 6, assuming partial penetration and pure adsorption, respectively. The markers give the measured data points, the drawn line corresponds to the situation of pure adsorption, and the dashed line to that of partial penetration. The inset shows the result of the χ^2 analysis of the scattering length density of the lipid headgroup, which leads to a systematic error of $\pm 0.2 * 10^{-6}$ Å^{-2}.

region of the lipid layer. In all DIC-HIS experiments, the addition of protein causes a consistent reduction in the scattering length density of the hydrocarbon chain region ρ_1 of $\Delta\rho_1 = 0.1 * 10^{-6}$ Å^{-2} (cf. Table 3, column ρ_1). If we take the measured average area per DIC-HIS molecule of $A_P = 2800$ Å^2 and an area per lipid molecule of $A_L = 60$ Å^2, about one myristic acid chain of DIC-HIS should be present for every 47 phospholipid molecules. The incorporation of the protonated protein chain into the fully deuterated hydrocarbon region of the lipid should cause a decrease in scattering length density of $\Delta\rho_1 = 0.07 * 10^{-6}$ Å^{-2}, which is in good agreement with the measured change. However, because the change in ρ_1 is in the range of experimental accuracy, it is not possible to calculate a reliable value for the average area per DIC-HIS molecule from the decrease in the parameter ρ_1.

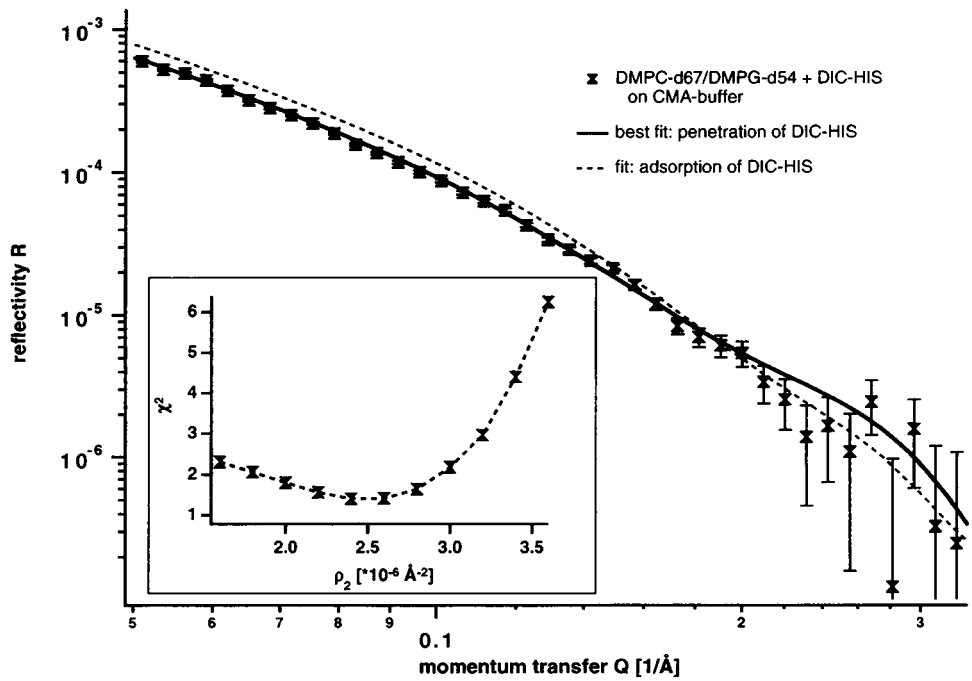

FIGURE 7 Comparison of optimal fits of $R(Q)$-versus-Q curves of DIC-HIS on 1:1 mixed DMPC-d67/DMPG-d54 monolayers on CMA buffer at pH 6, assuming partial penetration and pure adsorption, respectively. The markers give the measured data points, the drawn line corresponds to the situation of partial penetration, and the dashed line to that of pure adsorption. The inset shows the result of the χ^2 analysis of the scattering length density of the lipid headgroup, which leads to a systematic error of $\pm 0.2 * 10^{-6}$ Å^{-2}.

TABLE 4 Comparison of fitted parameters of layer thicknesses d_i, scattering length densities ρ_i, and interfacial roughnesses σ_i for DIC-HIS bound to 1:1 mixtures of DMPC-d67 and DMPG-54 in absence and presence of actin

Protein	Buffer	No. of layers	d_1 [Å]	ρ_1 [$*10^{-6}$ Å^{-2}]	σ_1 [Å]	d_2 [Å]	ρ_2 [$*10^{-6}$ Å^{-2}]	σ_2 [Å]
DIC-HIS pH 6	CMA	2	21	4.6	3	12	1.1	2
DIC-HIS + actin pH 6	CMA	2	23	4.0	3	54	0.1	10
DIC-HIS + actin pH 9	CMA	2	23	4.4	3	51	0.1	22
DIC-HIS pH 6	D_2O	2	14	5.4	3	25	5.9	3
DIC-HIS + actin pH 6	D_2O	2	14	5.2	3	63	6.0	12

Data are shown for CMA buffer at pH 6 and pH 9 and for D_2O buffer at pH 6.
In the case of D_2O buffer the indices 1 and 2 denote the layer of lipid chain and the layer consisting of lipid headgroup, DIC-HIS, and actin, respectively. For CMA-buffer the indices 1 and 2 denote the total lipid layer and the total protein layer consisting of DIC-HIS and actin, respectively.

Hisactophilin-mediated binding of G-actin

As shown in the previous publication by microfluorescence (Behrisch et al., 1995), natural hisactophilin can mediate the binding of monomeric actin to monolayers. However, this technique cannot distinguish between true binding and mere accumulation of proteins at the lipid/water interface. Therefore, we investigated the modification of the *R*-versus-*Q* curves for 1:1 mixtures of DMPC-d67/DMPG-d54 with bound natural hisactophilin (DIC-HIS) induced by the injection of G-actin into the subphase. For that purpose monomeric actin (42 kDa) was added to the subphase after equilibration of the hisactophilin binding to the monolayer at concentrations of DIC-HIS of 1.5 μg/ml (0.11 μM) and actin of 3.75 μg/ml (0.09 μM). To avoid polymerization of actin, Ca^{2+} in the subphase was sequestered by EGTA. Measurements were performed with both D_2O buffer and CMA buffer. The results of our analysis of the reflectivity curves are summarized in Table 4. For DIC-HIS on CMA, the indices 1 and 2 denote the total lipid layer and the total protein layer, consisting of DIC-HIS and actin, respectively. In the case of D_2O-contrasts the indices 1 and 2 correspond to the hydrophobic region of the lipid monolayer and the sum of lipid headgroup and total protein layer (DIC-HIS plus actin).

Fig. 8 shows reflectivity data (marker) of 1:1 mixed DMPC-d67/DMPG-d54 on the D_2O subphase after the addition of both DIC-HIS and G-actin together with the best fitting curve (*solid line*). In addition, the best fit (*dashed line*) describing the situation before the injection of actin is illustrated. The *R*(*Q*)-versus-*Q* plots in the absence and presence of actin differ remarkably. In particular, the reflectivity at $Q \leq 0.07$ Å^{-1} is reduced appreciably. Least-square fitting by a two-layer model shows that the thickness d_2, which comprises the headgroup and the protein layer, increases from $d_2 = 25 \pm 2$ Å in the absence to $d_2 = 63 \pm 2$ Å (cf. Fig. 8, *inset*) in the presence of actin (cf. Table 4),

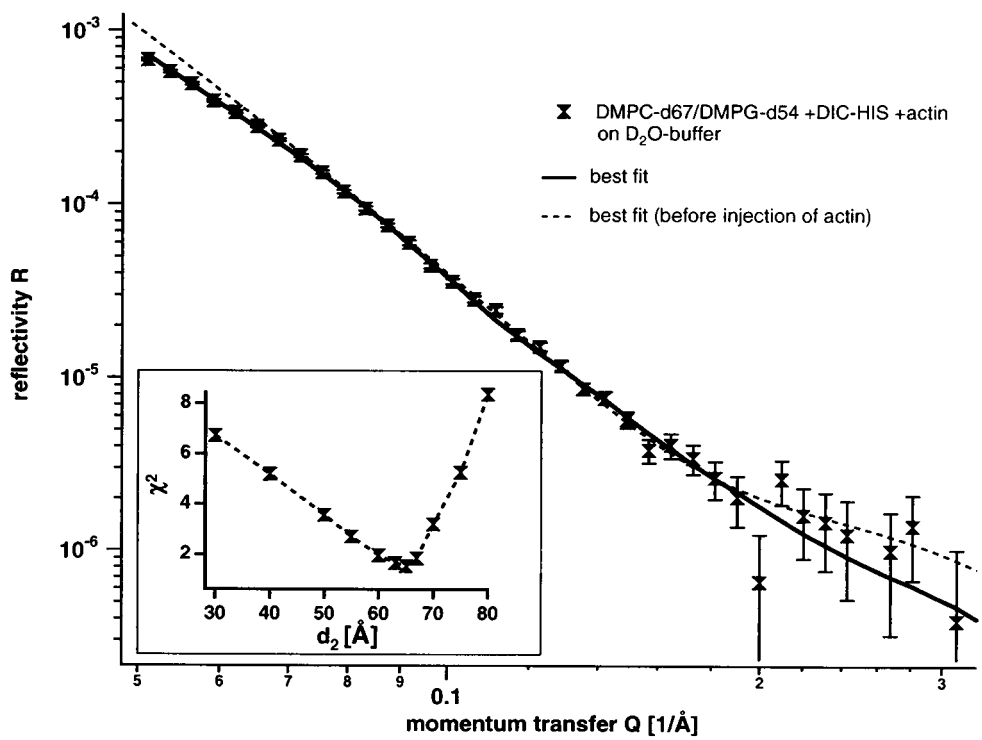

FIGURE 8 Plot of reflectivity *R*(*Q*) versus momentum transfer *Q* (marker) and corresponding fitting curve (solid line) of DIC-HIS bound to 1:1 mixed DMPC-d67/DMPG-d54 in the presence of 0.1 μM actin on CMA buffer at pH 6. The fitting curve obtained before injection of actin (dashed line) is shown for comparison. To simplify the representation, the data points obtained before injection of actin are not shown. A remarkable change is only observed at $Q < 0.07$ Å^{-1}. The inset illustrates the result of the χ^2 analysis of the layer thickness consisting of lipid headgroup and proteins (DIC-HIS plus actin), which leads to a systematic error of ±2 Å. Values of layer thicknesses d_i and scattering length densities ρ_i are summarized in Table 4.

while the scattering length density remains constant (ρ_2 = 6.0 ± 0.1 * 10^{-6} Å^{-2}) within experimental error. The increase in the thickness d_2 of about 40 Å due to actin adsorption agrees well with the thickness of the actin monomer, which is a globular protein of dimension 3.3 × 5 × 5.6 nm (Smith et al., 1983). This leads to the conclusion that actin forms a single monomolecular layer. From the values of total scattering length of the corresponding protein on D_2O-subphase b(protein), the fitted scattering length density ρ_P, the fitted thickness d_P, the scattering length density of D_2O $\rho(D_2O)$, and the area per protein molecule obtained by NMR-structure determination A_P(NMR), we can calculate the area occupied by one protein molecule A_P by the following equation:

$$A_P = A_P(\text{NMR}) + \frac{b(\text{protein}) - \rho_P d_P A_P(\text{NMR})}{\rho_P d_P - d_P \rho(D_2O)}. \quad (7)$$

First, we consider the DIC-HIS layer before the addition of actin. The theoretical scattering length of hisactophilin on the D_2O subphase can be estimated from structural data. The value of b(protein) ≈ 0.0525 Å leads to an area covered by one DIC-HIS molecule of A_P ≈ 5965 Å^2. Now, the fraction of the lipid area φ_P covered by DIC-HIS can be determined by using Eq. 6, which yields a value of about 18%. This result is in good agreement with the φ_P values found for the 1:1 mixtures of DMPC-d67/DMPG-d54 on the CMA subphase after the addition of DIC-HIS.

Second, we can now estimate the area covered by one actin molecule in the same manner. Together with the theoretical scattering length of actin on the D_2O subphase of b(protein) ≈ 0.242 Å and an averaged area of 1200 Å^2 from x-ray structural data, one obtains from Eq. 7 an area per actin molecule of A_P ≈ 9026 Å^2. Using Eq. 6 and taking into account a maximum area of actin of 1650 Å^2, we can now calculate the fraction of lipid area φ_P covered by actin. A value of about 18% is found. The agreement of the φ_P values of DIC-HIS and actin shows that 65% of the membrane-bound DIC-HIS are coupled to one actin molecule, because the molecular areas of DIC-HIS (~1000 Å^2) and actin (~1500 Å^2) are similar. It means that the histidine-rich loops of DIC-HIS, which are the only binding sides for the actin molecule, should mainly point into the subphase.

A more careful analysis of the actin experiments shows that the reflectivity data can only be fitted in a satisfactory way by considering an interfacial roughness σ_i as an additional parameter for each layer. Our fitting procedure yields σ_1 = 3 ± 3 Å and σ_2 = 12 ± 3 Å. For comparison, we also determined values of roughness for the case of the actin free monolayer, for which we find σ_1 = 3 ± 3 Å and σ_2 = 3 ± 3 Å. The roughness of the lipid layer is of the order of the resolution limit and thus is insignificant. However, the roughness caused by actin binding is much larger than the resolution limit, strongly suggesting that the interfacial roughness between actin and subphase is remarkably increased. As illustrated in Fig. 9, our findings are also supported by the χ^2 analysis of σ_2, which yields in the case of actin χ^2 = 2.2 for σ_2 = 0 Å and χ^2 = 1.46 for σ_2 = 12 Å.

In the case of CMA buffer, the changes in the reflectivity behavior are much less pronounced. Therefore, the data (not shown) were only analyzed in terms of a two-layer model composed of a lipid layer and a protein layer. The total protein layer thickness of d_2 = 54 ± 4 Å (cf. Table 4) can be interpreted as the superposition of a 12-to 15-Å-thick layer of hisactophilin and a 40-Å-thick actin layer. However, these results represent a rather crude estimation, because the scattering contrast between protein layer and the CMA subphase is in the range of the experimental accuracy (ρ_2 = 0.1 ± 0.1 * 10^{-6} Å^{-2}). To optimize the fitting results,

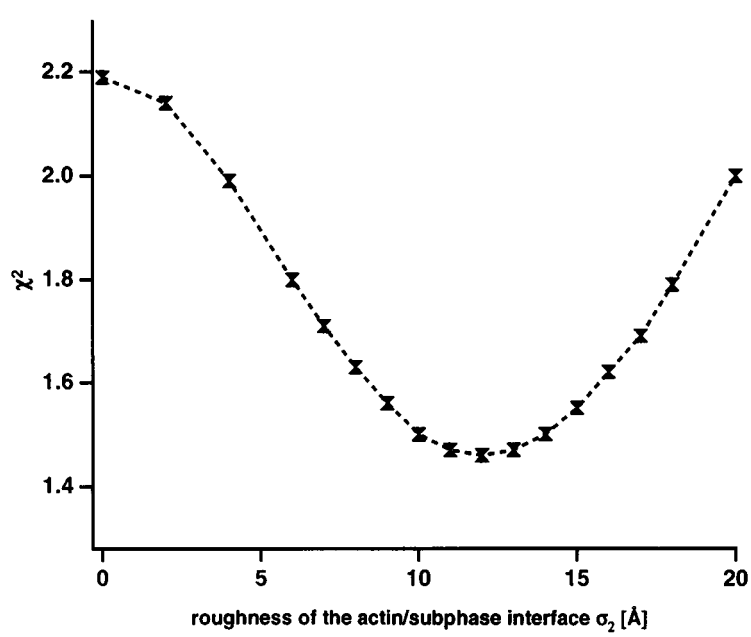

FIGURE 9 Plot of χ^2 versus interfacial roughness of the actin/subphase interface σ_2, which leads to the statistical error of $\Delta\sigma_2$ = ±3 Å. This supports the idea that in contrast to the flat interface between hisactophilin and subphase ($\sigma_2 \leq 3$ Å), the interface between actin and subphase (σ_2 = 12 Å) is rather rough (cf. Table 4).

we had to include interfacial roughness again. Before the addition of actin, we obtain $\sigma_1 = \sigma_2 = 3 \pm 3$ Å, whereas $\sigma_1 = 3 \pm 3$ Å and $\sigma_2 = 10 \pm 3$ Å in the presence of actin. This is in good agreement with the results obtained for the D_2O subphase.

In a separate experiment, we studied the modification of the reflectivity curve of the DMPC/DMPG/DIC-HIS/G-actin layer by changing the pH of the CMA subphase from pH 6 to pH 9 (lines 3 and 4 in Table 4). According to Table 4, the thickness d_2 of the layer attributed to the adsorbed proteins does not change remarkably. The invariance of d_2 is surprising, because it is well known (cf. Scheel et al., 1989; Behrisch et al., 1995) that the binding of actin by hisactophilin is suppressed at pH > 8. Moreover, owing to the neutralization of the histidine groups at pH > 8, the electrostatic binding of the protein to the monolayer is expected to be reduced. On the other hand, the data indicate that the binding strength of actin is appreciably reduced. The scattering length density ρ_1 attributed to the lipid layer increases from $\rho_1 = 4.0 \pm 0.2 * 10^{-6}$ Å^{-2} at pH 6 to $\rho_2 = 4.4 \pm 0.2 * 10^{-6}$ Å^{-2} at pH 9. The latter approaches this value in the absence of both hisactophilin and actin ($\rho_2 = 4.6 \pm 0.2 * 10^{-6}$ Å^{-2}), indicating a weaker coupling of the proteins with the lipid monolayer. The weaker actin-hisactophilin coupling is also supported by the increase in the roughness σ_2 from 10 Å at pH 6 to 22 Å at pH 9 (cf. Table 4). As will be discussed in the next section, the small effect of the histidine neutralization could be rationalized in terms of hysteresis effects or in terms of a change of the pK value of the protein. Such changes of pK at the air/water interface have been well established for partially charged lipid layers.

DISCUSSION

The present experiments demonstrate that neutron reflectivity measurements and their evaluation in terms of the classical model of specular reflection at stratified layers provides a technique for studying the adsorptive interaction of proteins with membranes. In fact, as shown previously (Johnson et al., 1991a), the technique may be easily extended to supported bilayers, which are more realistic models of biomembranes than monolayers. The latter, however, have the major advantage of controlling the lateral pressure.

In our previous film balance and microfluorescence studies, we showed that both the natural (DIC-HIS) and the fatty acid-depleted (EC-HIS) hisactophilin bind strongly to partially charged membranes of DMPC/DMPG mixtures and weakly to DMPC at lateral pressures up to 30 mN/m. These experiments suggested, moreover, that both species bind to the monolayer, leading to lateral condensation of the lipid. Together with the previous studies (Behrisch et al., 1995), the present neutron reflectivity measurements suggest the models shown in Fig. 10, which stresses our finding that only the protein with the myristic acid chain actually penetrates into the lipid monolayer.

According to Table 3, the scattering length density of the lipid headgroup for the CMA buffer is decreased by about 30% (from $\rho_2 = 3.5 \pm 0.2 * 10^{-6}$ Å^{-2} to $\rho_2 = 2.5 \pm 0.2 * 10^{-6}$ Å^{-2}). This strongly suggests that the natural protein DIC-HIS penetrates with amino acid side chains into the semipolar region of the lipid monolayer. A remarkable result is that this interaction mechanism is similar for charged and noncharged lipid layers. Additionally, our experimental results indicate a partial penetration of the myristic chain of DIC-HIS into the hydrocarbon interior of the lipid layer, although the degree of penetration is astonishingly small.

Judged from the present studies it appears that the electrostatic interaction increases the local concentration of the protein near the surface of the lipid, and the binding equilibrium of hisactophilin to the membrane is therefore expected to be shifted toward the side of the bound protein.

The previous monolayer experiments (Behrisch et al., 1995) and the present study provide evidence that the fatty acid is important for the hisactophilin-mediated binding of actin to membranes and suggest a different orientation of the DIC-HIS and EC-HIS for the following reasons.

First, one knows from biochemical studies that the charged histidine groups are necessary for the binding of actin, suggesting that they provide the tight binding places

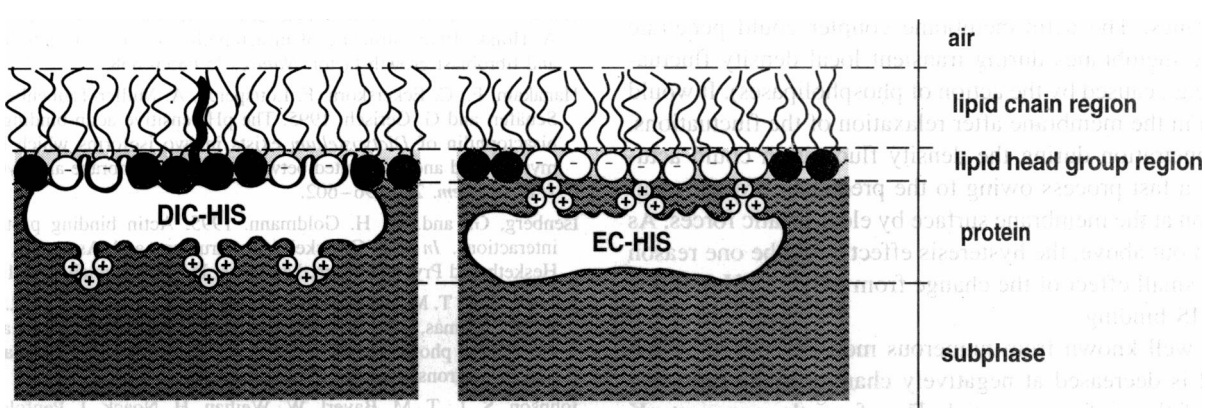

FIGURE 10 Schematic view of models of different binding of natural DIC-HIS (*left*) and fatty acid-deficient (genetic product) EC-HIS (*right*) coupled to a partially charged DMPC/DMPG mixed monolayer.

for actin-hisactophilin coupling (Scheel et al., 1989). Moreover, EC-HIS promotes the polymerization and bundling of actin filaments, as suggested by quasielastic light scattering experiments (R. Götter and E. Sackmann, unpublished results).

Second, the monolayer experiments clearly showed that EC-HIS cannot mediate the binding of actin monomers to the membrane, but that it induces the polymerization of actin under nonpolymerizing conditions (Behrisch et al., 1995) with long polymers penetrating into the subphase. It is for that reason that we did not study the EC-HIS/actin system by neutron reflectivity measurements, because the scattering length densities of actin and water are so similar (no contrast) that the diffuse actin layer would not be detectable.

The most likely explanation for the above finding is that actin competes with the lipids for the histidine-rich binding places of hisactophilin and displaces EC-HIS from the monolayer, suggesting that the histidine groups are in more intimate contact with the monolayer than in the case of DIC-HIS.

The present work has provided further and more direct evidence that actin-binding proteins can mediate the binding of actin to lipid membranes at high lateral pressures (~25 mN/m) similar to those in biological membranes. Moreover, we demonstrated that the fatty acid anchor is essential for the tight binding and the functional orientation of the membrane-associated proteins. The charged lipids strongly favor the protein binding but are not absolutely necessary. As shown in the previous film balance experiments, the fraction of bound protein increases rapidly with increasing content of charged lipid (DMPG) but is already saturated at 30 mol% of DMPG, which is remarkably close to the lipid content in the inner monolayer of the plasma membrane.

Judged from the film balance experiments, hisactophilin does not penetrate into monolayers at lateral pressures $\pi \geq$ 30 mN/m (Behrisch et al., 1995). However, we also showed in the previous paper that once the protein is incorporated at lower π values ($\pi \leq 25$ mN/m), it remains in the membrane up to 35 mN/m before it is squeezed out. This strong hysteresis provides a possible mechanism for the control of hisactophilin-mediated coupling of actin to intracellular membranes. The actin-membrane coupler could penetrate into the membranes during transient local density fluctuations (e.g., caused by the action of phospholipases). It would remain in the membrane after relaxation of the fluctuations. The penetration during the density fluctuation could actually be a fast process owing to the preceding protein accumulation at the membrane surface by electrostatic forces. As pointed out above, the hysteresis effect could be one reason for the small effect of the change from pH 6 to pH 9 on the DIC-HIS binding.

It is well known from numerous monolayer studies that the pH is decreased at negatively charged membranes because of the surface potential. Therefore, the apparent pK values of lipids or other charged species adsorbed to acidic monolayers are higher than the value found in the bulk phases. The present experiments were performed at an ionic strength of about 20 mM, corresponding to a Debye screening length of $\kappa^{-1} \approx 20$ Å. Because the measured thickness of hisactophilin is about 15 Å, the histidine groups would feel a strong negative potential, even if the histidine groups are pointing away from the monolayer surface. For that reason the difference in the binding strengths of DIC-HIS and EC-HIS is expected to be small at low ionic strengths.

The present work demonstrates that neutron surface scattering techniques provide a powerful tool for detailed studies of protein-membrane interaction and protein-protein recognition at membranes. In particular, it can be applied to the large class of nonintegral but membrane-associated proteins, which couple to lipid layers by the combination of electrostatic or/and hydrophobic forces (in the presence of fatty acid chains). These include phospholipases, kinases, G-proteins, or cell contact site proteins of *Dictyostelium* cells. Because many of these proteins are only available in small quantities, the high sensitivity of the present technique is a great advantage.

REFERENCES

Als-Nielsen, J. 1985. The liquid vapour interface. *Z. Phys. B-Condensed Matter.* 61:411–414.

Bayerl, T. M., R. K. Thomas, J. Penfold, A. R. Rennie, and E. Sackmann. 1990. Specular reflection of neutrons at phospholipid monolayers. Changes of monolayer structure and head group hydration at the transition from the expanded to the condensed phase state. *Biophys. J.* 57:1095–1098.

Behrisch, A., Ch. Dietrich, A. A. Noegel, M. Schleicher, and E. Sackmann. 1995. Actin binding protein hisactophilin binds to partially charged membranes and mediates actin coupling to membranes. *Biochemistry.* 34:15182–15190.

Born, M., and E. Wolf. 1970. Principles of Optics. Pergamon Press, Oxford.

Brumm, T., C. Naumann, E. Sackmann, A. R. Rennie, R. K. Thomas, D. Kanellas, J. Penfold, and T. M. Bayerl. 1994. Conformational changes of the lecithin head group in monolayers at the air/water interface. A neutron reflection study. *Eur. Biophys. J.* 23:289–296.

Dietrich, C., W. H. Goldmann, E. Sackmann, and G. Isenberg. 1993. Interaction of NBD-talin with lipid monolayers, a film balance study. *FEBS Lett.* 324:37–40.

Goldmann, W. H., A. Bremer, M. Häner, U. Aebi, and G. Isenberg. 1994. Native talin is a dumbbell-shaped homodimer when it interacts with actin. *J. Struct. Biol.* 112:3–10.

Habazettl, J., D. Gondol, R. Wiltscheck, J. Otlewski, M. Schleicher, and T. A. Holak. 1992. Structure of hisactophilin is similar to interleukin-1b and fibroblast growth factor. *Nature.* 359:855–858.

Hanakam, F., C. Eckerskorn, F. Lottspeich, A. Müller-Taubenberger, W. Schäfer, and G. Gerisch. 1995. The pH-sensitive actin-binding protein hisactophilin of *Dictyostelium* exists in two isoforms which both are myristylated and distributed between plasma membrane and cytoplasm. *J. Biol. Chem.* 270:596–602.

Isenberg, G., and. W. H. Goldmann. 1995. Actin binding protein-lipid interactions. *In* The Cytoskeleton: Structure and Assembly, Vol. 1. Hesketh and Pryme, editors. JAI Press, Inc., Greenwich, CT. 169–204.

Johnson, S. J., T. M. Bayerl, D. C. McDermott, G. W. Adam, A. R. Rennie, R. K. Thomas, and E. Sackmann. 1991a. Structure of an adsorbed dimyristoyl phosphatidylcholine bilayer measured with specular reflection of neutrons. *Biophys. J.* 59:289–294.

Johnson, S. J., T. M. Bayerl, W. Weihan, H. Noack, J. Penfold, R. K. Thomas, D. Kanellas, A. R. Rennie, and E. Sackmann. 1991b. Coupling of spectrin and polylysine to phospholipid monolayers studied by specular reflection of neutrons. *Biophys. J.* 60:1017–1025.

Kaufmann, S., J. Käs, W. H. Goldmann, E. Sackmann, and G. Isenberg. 1992. Talin anchors and nucleates actin filaments at lipid membranes: a direct demonstration. *FEBS Lett.* 314:203–205.

Naumann, C., T. Brumm, A. R. Rennie, J. Penfold, and T. M. Bayerl. 1995. Hydration of DPPC monolayers at the air/water interface and its modulation by the nonionic surfactant $C_{12}E_4$: a neutron reflection study. *Langmuir.* 11:3948–3952.

Naumann, C., C. Dietrich, J. R. Lu, R. K. Thomas, A. R. Rennie, J. Penfold, and T. M. Bayerl. 1994. Structure of mixed monolayers of DPPC and polyethylene glycol monododecyl ether at the air/water interface determined by neutron reflection and film balance techniques. *Langmuir.* 10:1919–1925.

Penfold, J., and R. K. Thomas. 1989. The Application of the specular reflection of neutrons to the study of surfaces and interfaces. *Sci. Eng. Res. Council RAL.* 57:1–72.

Penfold, J., R. C. Ward, and W. G. Williams. 1987. A time of flight neutron reflectometer for surface and interfacial studies. *J. Phys. E. Sci. Instrum.* 20:1411.

Russell, T. P. 1990. X-ray and neutron reflectivity for investigation of polymers. *Mater. Sci. Rep.* 5:171–271.

Samuels, M., R. M. Ezzell, T. J. Cardozo, D. R. Critchley, J.-L. Coll, and E. Adamson. 1993. Expression of chicken vinculin complements the adhesion-defective phenotype of mutant mouse F9 embryonal carcinoma cell. *J. Cell Biol.* 121:909–921.

Scheel, J., K. Ziegelbauer, Th. Kupke, B. M. Humbel, A. A. Noegel, G. Gerisch, and M. Schleicher. 1989. Hisactophilin, a histidine-rich actin-binding protein from *Dictyostelium discoideum*. *J. Biol. Chem.* 264: 2832–2839.

Smith, P. R., W. E. Fowler, T. D. Pollard, and U. Aebi. 1983. Structure of the actin molecule determined from electron micrographs of crystalline actin sheets with a tentative alignment of the molecule in the actin filament. *J. Mol. Biol.* 167:641–660.

Vaknin, D., K. Kjaer, J. Als-Nielsen, and M. Lösche. 1991. Structural properties of phosphatidylcholine in a monolayer at the air/water interface. *Biophys. J.* 59:1325–1332.